

## Convective generation of cirrus near the tropopause

T. J. Garrett,<sup>1</sup> A. J. Heymsfield,<sup>2</sup> M. J. McGill,<sup>3</sup> B. A. Ridley,<sup>2</sup> D. G. Baumgardner,<sup>4</sup>  
T. P. Bui,<sup>5</sup> and C. R. Webster<sup>6</sup>

Received 23 April 2004; revised 16 June 2004; accepted 20 July 2004; published 6 November 2004.

[1] During the July 2002 CRYSTAL-FACE field program based from Key West, Florida, aircraft measurements showed that long-lived thin tropopause cirrus (TTC) layers were often present above thunderstorm anvils. This paper describes these clouds and explores their possible origins. Measurements showed that the horizontal dimensions of TTC layers were nearly identical to convectively formed anvils beneath, but that TTC did not appear to have originated from convective detrainment. Rather, they appeared to have formed in stably stratified air derived from high altitudes near the tropopause. TTC were separated vertically from the top of the anvil by  $\sim 1$  km, they lacked precipitation particles, and they were strongly depleted in HDO, all of which indicate in situ formation. However, compared to surrounding clear air near the tropopause, TTC were enriched in moisture and trace gases. The degree of enrichment was consistent with mixing of air near the tropopause with the same convective air mass that produced the anvil. Unlike surrounding air, TTC had embedded a monochromatic gravity wave with a wavelength of 2 km and an amplitude of several hundred meters. This evidence, supported by a photograph from CRYSTAL-FACE, leads to the conjecture that TTC originate as stratiform pileus clouds that form near the tropopause ahead of vigorous convective uplift. We hypothesize that the pileus are penetrated by the convection, moistened through turbulent mixing, and once the convection subsides, they are sustained by radiative cooling due to the presence of the anvil layer beneath. *INDEX TERMS:* 0320 Atmospheric Composition and Structure: Cloud physics and chemistry; 0322 Atmospheric Composition and Structure: Constituent sources and sinks; 3314 Meteorology and Atmospheric Dynamics: Convective processes; *KEYWORDS:* tropopause cirrus, anvil cirrus, convection

**Citation:** Garrett, T. J., A. J. Heymsfield, M. J. McGill, B. A. Ridley, D. G. Baumgardner, T. P. Bui, and C. R. Webster (2004), Convective generation of cirrus near the tropopause, *J. Geophys. Res.*, 109, D21203, doi:10.1029/2004JD004952.

### 1. Introduction

[2] Within a “tropical tropopause layer” (TTL) located near or within the tropopause, air is decoupled from the convection dominated lower troposphere. Here tenuous layers of cirrus are often found. Since these cirrus layers are both widespread and very cold, they have attracted considerable interest for their contributions to the atmospheric greenhouse effect and for their hypothesized role toward the dehydration of the lower stratosphere.

[3] Thin cirrus near the tropopause have been characterized in situ by aircraft [Heymsfield, 1986; McFarquhar *et al.*, 2000; Pfister *et al.*, 2001; Luo *et al.*, 2003; Santacesaria

*et al.*, 2003], from space using IRIS and MODIS satellite imagery [Prabhakara *et al.*, 1988; Dessler and Yang, 2003], lidar and limb scanner imagery from the space shuttle [Winker and Trepte, 1998; Spang *et al.*, 2002], and by ground-based lidar [Sunil Kumar *et al.*, 2003]. The lidar measurements show cloud layers located against the lower bound of the tropopause between about 14 and 16 kilometers altitude in layers a few hundred meters to 1 kilometer thick, and with large horizontal extent, ranging up to 2700 km across [Winker and Trepte, 1998; Sunil Kumar *et al.*, 2003].

[4] Tropopause cirrus have been subclassified into “thin tropopause cirrus” (TTC), with optical depths  $\tau < 0.3$ , “subvisible cirrus” (SVC), invisible to the naked eye with  $\tau < 0.03$ , and even ultrathin tropopause cirrus” (UTTC) with  $\tau \sim 10^{-4}$ , recently observed over the western Indian Ocean by Luo *et al.* [2003]. Likely all these cloud types are manifestations of the same physical phenomenon [Santacesaria *et al.*, 2003]. Uniformly, observations show that the sizes of ice crystals in these cirrus layers are extremely small, with mean diameters ranging from 5 to 25  $\mu\text{m}$  diameter [Prabhakara *et al.*, 1988; McFarquhar *et al.*, 2000; Luo *et al.*, 2003]. The shapes of the ice crystals are primarily trigonal and columnar [Heymsfield, 1986].

<sup>1</sup>Meteorology Department, University of Utah, Salt Lake City, Utah, USA.

<sup>2</sup>National Center for Atmospheric Research, Boulder, Colorado, USA.

<sup>3</sup>NASA Goddard Space Flight Center, Greenbelt, Maryland, USA.

<sup>4</sup>Centro de Ciencias de la Atmosfera, Universidad Nacional Autonoma de Mexico, Mexico City, Mexico.

<sup>5</sup>NASA Ames Research Center, Moffett Field, California, USA.

<sup>6</sup>Earth and Space Sciences Division, Jet Propulsion Laboratory, California Institute of Technology, Pasadena, California, USA.

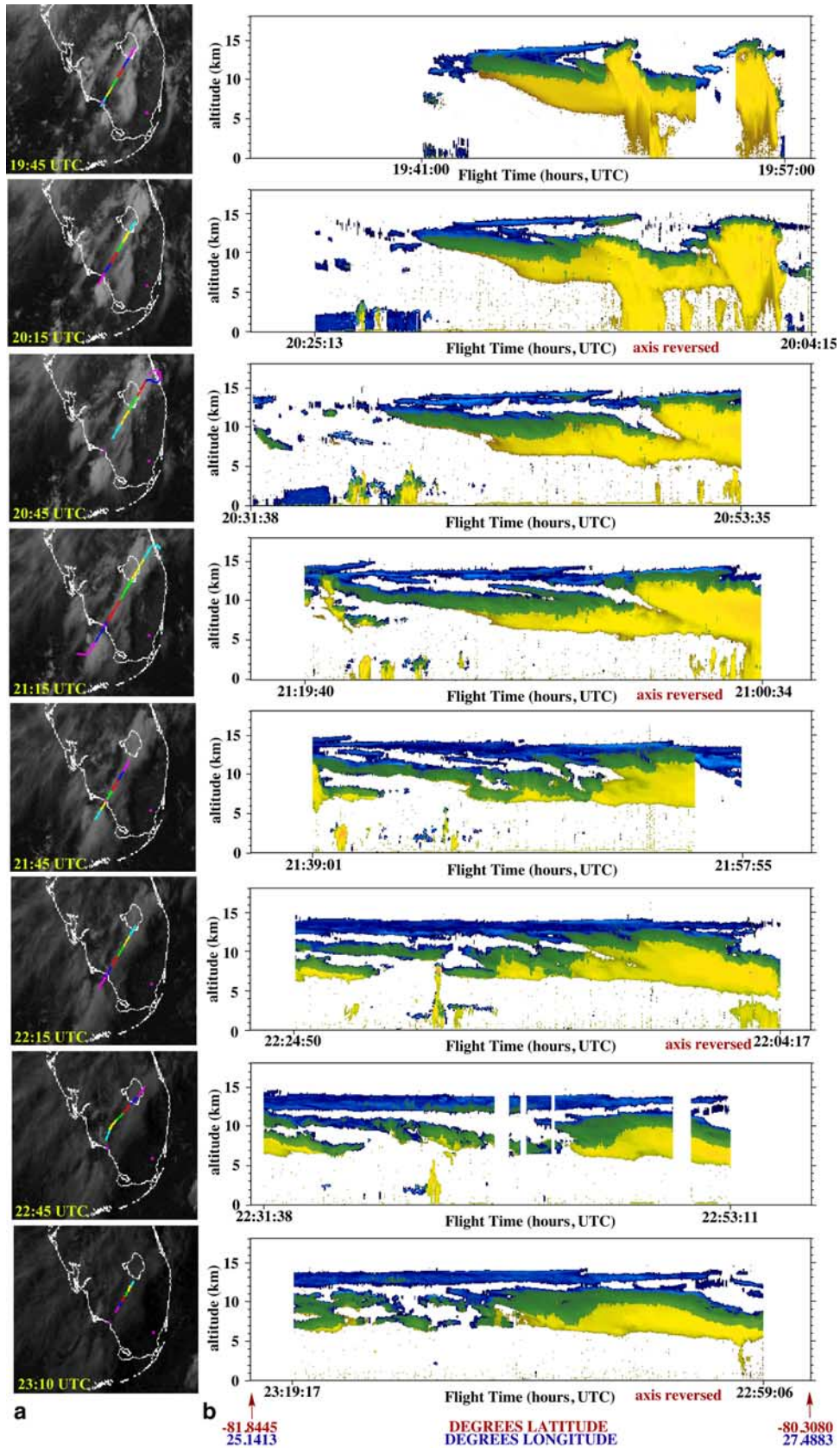


Figure 1

[5] *Santacesaria et al.* [2003] estimated that TTC reduce outgoing infrared flux by 10%, while *McFarquhar et al.* [2000], based on three clouds measured in situ, estimated that thinner SVC reduce net outgoing flux by an average  $1.6 \text{ W m}^{-2}$ . They point out that, while such forcing is small, it is important in light of the delicate balance in the tropics between longwave warming and shortwave cooling. *McFarquhar et al.*'s [2000] calculations also showed SVC heating the upper troposphere heating by 1.7 K/day. Modeling studies by *Jensen et al.* [1996a] suggest that under conditions of gentle ascent, tropopause cirrus might precipitate, in which case local heating could loft the desiccated layer into the lower stratosphere. They suggested this might explain observations of extraordinary low stratospheric humidity.

[6] What remains uncertain is the origin of tropopause cirrus. *Jensen et al.* [1996b] showed that anvil outflow from deep convection leaves behind only a tenuous layer of small ice crystals once bigger particles have precipitated. Alternatively, they argued, synoptic-scale lifting of a moist layer creates ice supersaturations sufficient to induce homogeneous nucleation of ice crystals from preexisting haze particles. In both scenarios, the cloud might persist for days provided infrared absorption by the cloud layer drives lofting of the layer rather than local heating. Thirdly, lifting might be forced by convection. *Potter and Holton* [1995] showed that deep convective storms create vertically propagating buoyancy waves that extend upwind of the convection into the lower stratosphere. These waves have horizontal wavelengths of 70 km and vertical displacements of several hundred meters. In the upward phase of these waves tenuous cloud layers may form. Similarly, *Boehm and Lee* [2003] suggested that vertical motions that form cirrus in the TTL are Rossby waves forced by meridional circulations due to deep convection.

[7] Most observations show that both convection and synoptic-scale uplift play a role in thin cirrus formation. However, while many suggest their formation in the tropics is associated primarily with convective outflow [*Prabhakara et al.*, 1988; *Pfister et al.*, 2001; *Spang et al.*, 2002; *Dessler and Yang*, 2003], others point out that synoptic-scale uplift plays an equal if not dominant role [*Massie et al.*, 2002; *Sunil Kumar et al.*, 2003]. *Pfister et al.* [2001] argued that some thin cirrus formed in situ resembles synoptic-scale gravity waves that may have been generated by convection. An alternative hypothesis proposed by *Santacesaria et al.* [2003] is that cumulonimbus induced wave activity produces a turbulent mixed layer that leads to the upward transport of water vapor near the tropopause, hence leading to cloud formation. Regardless of the formation mechanism, preexisting high upper troposphere relative humidities aid thin cirrus formation and prolong their lifetimes by reducing the

degree of lifting required to increase haze aerosol activity to the point of homogeneous freezing [*Jensen et al.*, 1999; *Sandor et al.*, 2000].

[8] Tropical tropopause and anvil cirrus have been observed stacked above one another, vertically separated by several kilometers [*Winker and Trepte*, 1998; *Santacesaria et al.*, 2003]. T. J. Garrett et al. (Evolution of a Florida cirrus anvil, submitted to the *Journal of Atmospheric Sciences*, 2004) (hereinafter referred to as Garrett et al., submitted manuscript, 2004) presented a case study associated with a single isolated storm observed on 21 July 2002 during the Cirrus Regional Study of Tropical Anvils and Cirrus Layers-Florida Area Cirrus Experiment (CRYSTAL-FACE). CRYSTAL-FACE was focused on low-latitude cirrus anvils over a  $3^\circ \times 3^\circ$  domain southwest of  $27^\circ\text{N}$   $80^\circ\text{W}$  during July 2002. Garrett et al. (submitted manuscript, 2004) used aircraft data to study the evolution of the 21 July case, and found that cloudy air downwind of the convection was separable into the anvil proper with a TTC layer aloft. Over three hours, the anvil dissipated while the TTC cloud persisted.

[9] Further investigation showed that this scenario was in fact common over the course of CRYSTAL-FACE, with clear examples seen on most flights, including 9, 11, 16, 21, 23, and 28 July. The aircraft that sampled these clouds in situ during CRYSTAL-FACE, the NASA WB-57F, was outfitted with an unprecedented array of instruments for measuring the chemical and physical properties of high altitude clouds. Further, the WB-57F often flew in coordination with an ER-2 aircraft, which used remote sensing instruments to study convective clouds from above. In this paper we use measurements from these aircraft to describe tropopause cirrus above anvils and assess their origins. The analysis leads to a hypothesis that, over low-latitude deep convection, tropopause cirrus originate as stratiform pileus clouds forced by convective uplift.

[10] In section 2 we examine the structural and dynamic properties of the TTC layer. Section 3 discusses their microphysical and chemical properties. These measurements are discussed in section 4, where the origins of these TTC layers are examined. The paper's summary is presented in section 5.

## 2. Structural Properties

### 2.1. Cloud Vertical Structure and Evolution

[11] On 23 July 2002, the ER-2 flew 8 consecutive flight segments back-and-forth along the same coordinates in an intentional effort to map the evolution of a cirrus anvil [*McGill et al.*, 2004]. Downward looking 532 nm Cloud Physics Lidar (CPL) [*McGill et al.*, 2002] and 94 GHz Cloud Radar System (CRS) [*Li et al.*, 2004] imagery are combined to provide a detailed image of cloud structure

**Figure 1.** Evolution of a single cirrus anvil observed on 23 July 2002, measured with combined 532 nm lidar (CPL) and 94 GHz radar (CRS) from the ER-2 aircraft. (a) Visible images from the GOES satellite. Each image is approximately centered on the corresponding CPL image. (b) Combined CPL and CRS profiles. Blue shading indicates cloudy layers where a signal was present only in the CPL data. Yellow shading shows layers seen only in the CRS data. Green shading represents regions where both CPL and CRS detected layers. (c) Lidar-derived optical depth  $\tau$  for the cirrus layers. Red dots are optical depth of the upper layer (the TTC) in areas where the TTC is distinctly separated from underlying cloud. Blue dots are optical depth of the entire cirrus layer up to the limit of signal attenuation ( $\tau \approx 3$ ).

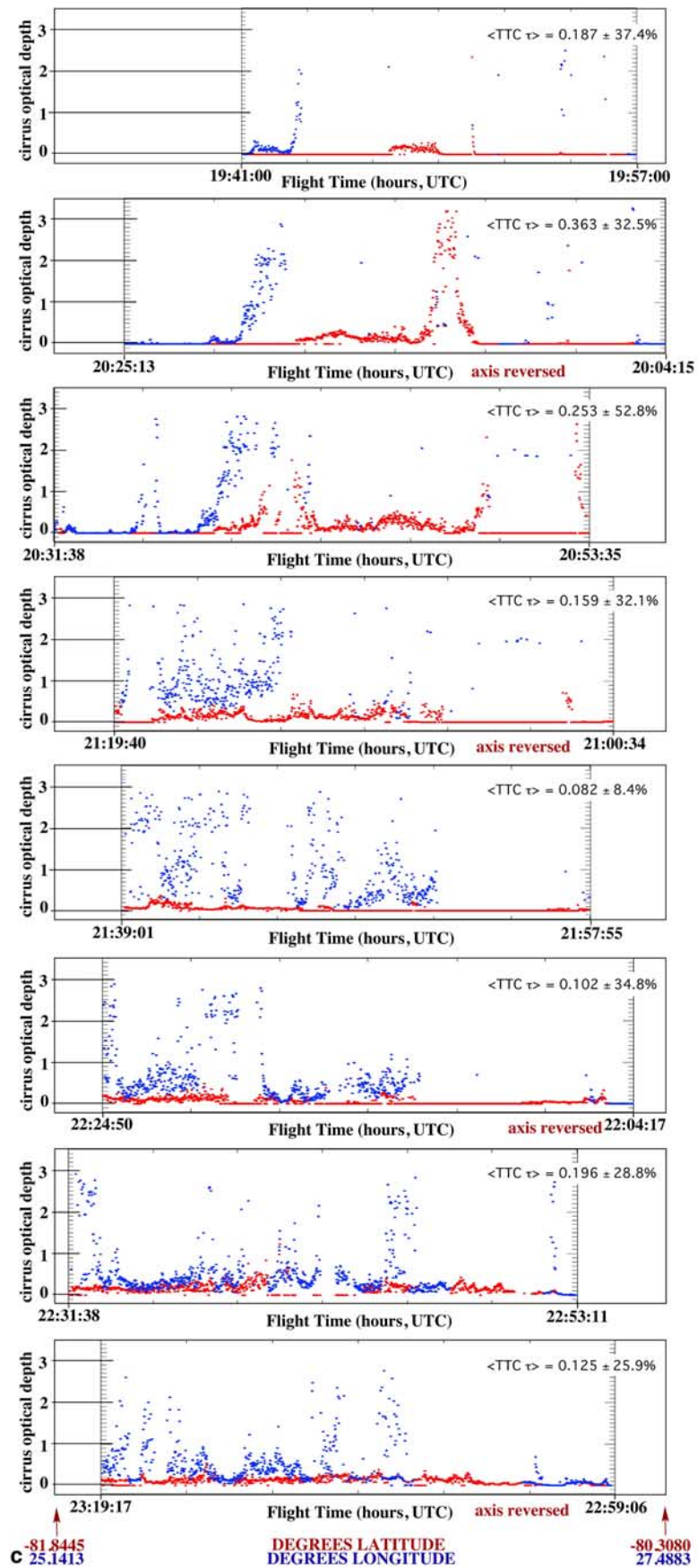
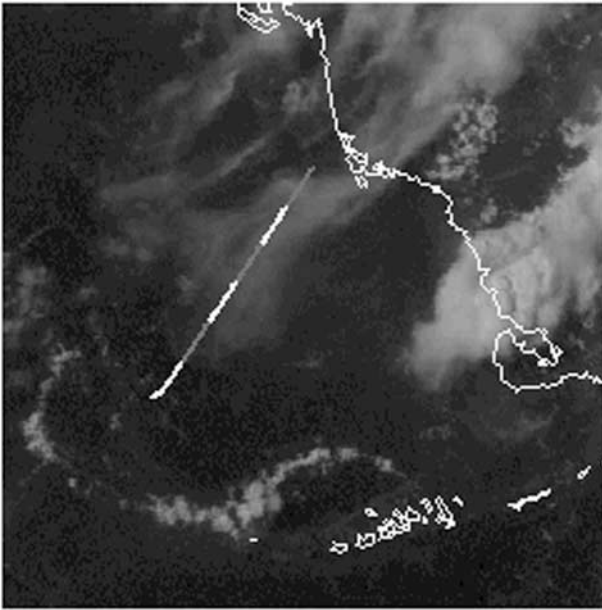


Figure 1. (continued)



**Figure 2.** WB-57 flight transect on 21 July 2002 in thin tropopause cirrus across the dimensions of the anvil visible beneath. The flight path, from northeast to southwest, covered the period 72600 to 73260 UTC (2010 to 2021 UTC), shown in approximately 2 min segments.

(Figure 1a–1c). The lidar is sensitive to small ice crystals, but is attenuated rapidly by clouds, whereas the radar has a larger penetration depth, but is sensitive primarily to precipitation sized ice crystals. The combined profiles are color coded such that yellow shading indicates cloud layers detected only by the radar. Blue shading indicates cloud/aerosol layers detected only by the lidar, which is indicative of tenuous cloud composed primarily of ice crystals less than about  $100\ \mu\text{m}$  diameter. Green shading represents areas where both instruments simultaneously observed cloud. Thus the images provide a qualitative but highly visual indication of the structure of the anvil system.

[12] From the earliest stages, detrained cloud appears to have been divided into two layers: the anvil proper, with cloud tops around 12 kilometers, and a thin tropopause cirrus (TTC) layer with tops at 14.5 km. The TTC appears to have begun its formation on top of overshooting convective updrafts that reached their maximum altitude. It was initially only several hundred meters thick, and quickly settled by about 1 km once the convective turret subsided. In the following 3 hours the TTC evolved into an unbroken layer approximately 1.5 km thick and it settled an additional kilometer. The optical depth of the TTC was variable, but on average it was approximately 0.2 throughout the measurement time period. Vertically separated from the TTC was the optically thicker anvil cloud mass, which was detrained at lower levels from successive pulses of convection. After one hour, the anvil detached from the dissipating convection and became more uniform in depth along its length as it thinned and slowly broke up.

## 2.2. Horizontal Extent

[13] Figures 1a–1c show anvil and TTC evolution on 23 July during CRYSTAL-FACE. These measurements

were consistent with the microphysical and radiative evolution of another convective system sampled in situ on 21 July (Garrett et al., submitted manuscript, 2004). On this day also, a TTC layer was observed above an anvil layer. The TTC layer had an optical depth of approximately 0.2. This layer was too thin to be easily visually discernible in satellite imagery (Figure 2). However, thicker anvil cloud was clearly visible directly underneath.

[14] In a horizontal transect through the tenuous TTC layer, the WB-57F entered the upwind edge of the cloud at 2010 UTC, and exited the cloud at 2021 UTC. Since the aircraft flew at a speed of  $\sim 140\ \text{m s}^{-1}$ , this corresponded to a flight path in cloud of approximately 90 km. GOES 8 satellite retrievals of cloud optical depth  $\tau$  [Minnis et al., 1998] along the WB-57F flight path showed  $\tau$  increasing from 0 to  $\sim 3$  beginning at 2010 UTC, dropping to  $\tau \simeq 0.3$  at 2017 UTC (60 km downwind), and zero at 2020 UTC (80 km downwind). Thus the upwind edge of both the anvil and TTC had approximately the same location horizontally. Assuming the anvil was no longer beneath the WB-57F at 2017 UTC, the TTC extended approximately 30 km further downwind than the anvil.

[15] A similar example was seen on 9 July where the WB-57F flew through cirrus with temperatures of  $-75^\circ\text{C}$  at approximately  $16^\circ\text{N}$  (Figure 3). Rather than a single storm cell, as was seen in the 21 July case, organized convection produced a vast cirrus shield over Cape Gracias, Honduras. However here too, flight notes remarked that the layer in which the WB-57 flew was extremely thin and wispy, and that the thicker cirrus shield was below. Comparisons with GOES 8 satellite retrievals showed that the TTC layer had nearly identical horizontal dimensions to the thicker anvil layer beneath. An additional comparison made on 11 July gave the same conclusion. Similar comparisons were not possible on

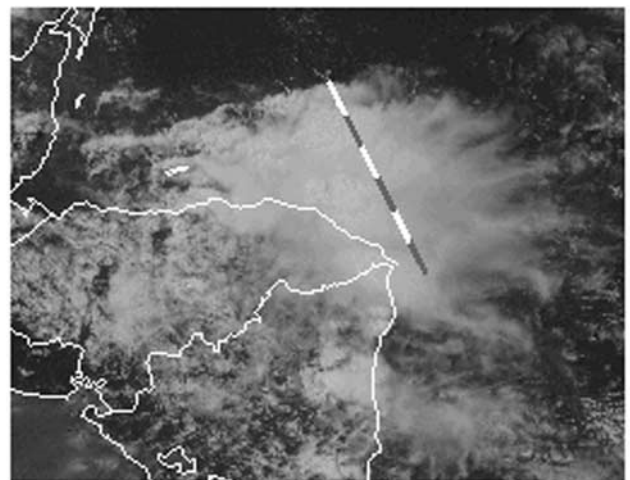


**Figure 3.** WB-57 flight transect on 9 July 2002 in thin tropopause cirrus across the dimensions of the anvil visible beneath. The flight path, from southeast to northwest, covered the period 66600 to 68400 UTC (1830 to 1900 UTC), shown in approximately 5 min segments.

**Table 1.** Boundaries of Anvil Cirrus and the Boundaries of Overlying Thin Tropopause Cirrus (TTC) Determined From in Situ Measurements From Aircraft Flying at  $\sim 140 \text{ m s}^{-1}$ <sup>a</sup>

	Anvil From Satellite, UTC	TTC From Aircraft, UTC
9 July	1823–1856	1827–1901
11 July	1850–1859	1846–1902
21 July	2010–2017	2010–2021

<sup>a</sup>Anvil cirrus is defined as where satellite retrievals showed  $\tau = 1$  provided the cloud top height  $> 8 \text{ km}$ . Tropopause cirrus is identified by its having an altitude higher than  $13.5 \text{ km}$ , an extinction coefficient  $\beta_{ext} < 1$ , and fractionation of HDO less than  $-200\%$ . See section 3 for measurement details. Boundaries are expressed in terms of the entrance and exit time along the aircraft flight path. Thus two clouds that overlay each other exactly along the aircraft flight path have the same entrance and exit times.

other days. The results for all these three cases on 9, 11, and 21 July are summarized in Table 1.

### 2.3. Gravity Waves

[16] Measurements of temperature obtained at 20 Hz ( $\sim 7 \text{ m}$  resolution) aboard the WB-57F using the Meteorological Measurement System [Scott *et al.*, 1990] are used here to explore the dynamic signature of tropopause cirrus cloud compared to ambient air. Data from the 21 July case are examined since they included two 10 min level flight passes at  $13.5 \text{ km}$ , flown along the downwind axis of the TTC, and 20 min flight in clear air nearby at the same altitude. Sufficient statistics were obtained to create a temperature power spectrum for wavelengths between  $14 \text{ m}$  and  $14 \text{ km}$  in both clear and cloudy air (Figure 4).

[17] The power spectral density for the potential temperature  $\theta$  was calculated using Welch’s averaged periodogram method for approximately 30 half overlapping 100 s blocks, subsequently averaged. The resulting temperature power spectra  $P_{\theta\theta}$ , calculated separately for clear and cloudy air, were subsequently divided by the square of the potential temperature gradient near the tropopause. This operation yields a power spectrum for buoyancy displacement in units of meters squared. Thus the calculated vertical amplitude of internal waves is

$$\delta z = \left( \frac{P_{\theta\theta}}{(d\theta/dz)^2} \right)^{1/2}$$

For clarity, the spectrum was averaged into 30 bins per wave number  $\kappa$ , where

$$\kappa = \frac{2\pi f}{tas}$$

and where  $f$  is the frequency of a particular spectral representation, and  $tas$  is the aircraft true airspeed.

[18] The wave number spectrum of  $\delta z^2$  is shown in Figure 4. There is a clear perturbation in the spectrum at  $\kappa = 0.003$  that is present in the tropopause cloud but not in surrounding clear air. This points to the presence of a gravity wave that was embedded in the cloud alone, which had an amplitude of  $\sim 200 \text{ m}$  and a wavelength of  $\sim 2 \text{ km}$ . In both spectra there is a peculiar “kink” at  $200 \text{ m}$  wavelength. Possibly this gap separates an internal

wave spectrum at lower wave numbers from a turbulent inertial subrange.

[19] Therefore it appears that the formation of the TTC cloud is related to a monochromatic gravity wave superimposed on an internal wave spectrum. This is discussed in relation to the cloud’s physical and chemical properties in section 4.

## 3. Physical and Chemical Properties

### 3.1. Measurements

[20] The WB-57F flew with a large suite of instrumentation for measuring the meteorological, microphysical, chemical and radiative properties of air in the upper troposphere and tropopause. Here we discuss the instrumentation and related parameters that are used in this study.

[21] In situ measurements of particle size distributions were obtained with a Cloud and Aerosol Particle Spectrometer (CAPS) [Baumgardner *et al.*, 2002]. Measurements of water vapor  $w$  and total water mixing ratios  $Q$ , from which the bulk ice water content  $IWC$  can be derived, were obtained using the Harvard Water Probe [Weinstock *et al.*, 1994]. The bulk cloud optical extinction coefficient  $\beta_{ext}$  was obtained using a Gerber Scientific Cloud Integrating Nephelometer [Gerber *et al.*, 2000]. Measurements of total water and its associated water isotopes were obtained from the Aircraft Laser Infrared Absorption Spectrometer (ALIAS) [Webster *et al.*, 1994]. Total water measurements from the Harvard Water Probe have received more extensive validation than those from the ALIAS, however the two probes were generally in good agreement during CRYSTAL-FACE. NO concentrations were obtained from an NO/NO<sub>y</sub> sensor [Ridley *et al.*, 2004].

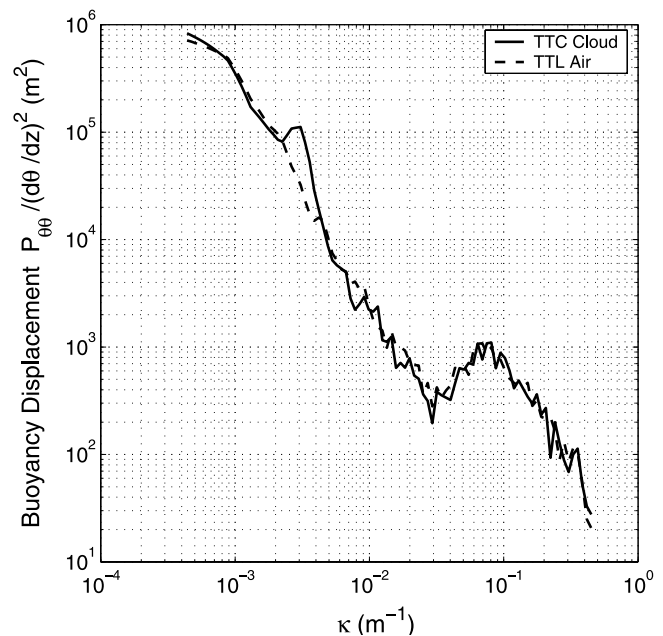


**Figure 4.** Buoyancy displacement (in  $\text{m}^2$ ) in clear and cloudy air derived from temperature measurements at  $13.5 \text{ km}$  altitude on 21 July 2002.

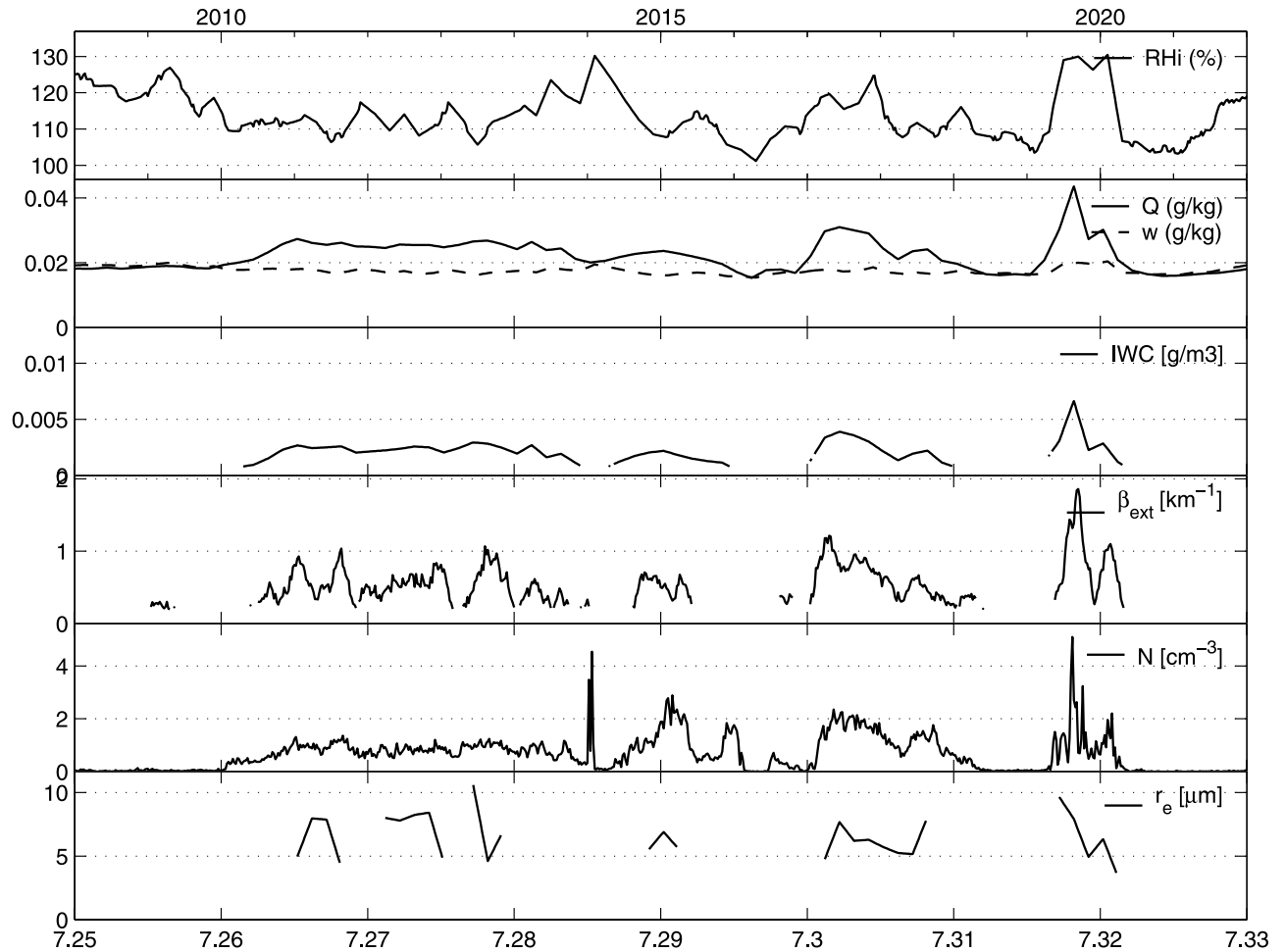


**Figure 5.** Time series of relative humidity over ice ( $RH_i$ ), total and water vapor mixing ratio ( $Q$  and  $w$ ), ice water content  $IWC$ , extinction coefficient  $\beta_{ext}$ , ice crystal concentration greater than  $2 \mu\text{m}$  diameter ( $N$ ), and ice crystal effective radius  $r_e$  derived from measurements of  $IWC$  and  $\beta_{ext}$  [Garrett et al., 2003], measured aboard the WB-57 on 21 July 2002 within tropopause cirrus at  $14.1 \text{ km}$  altitude. The direction of flight is from the cloud's upwind to downwind edge. Time on the bottom axis is in units of  $10^4 \text{ s UTC}$ . Measurements correspond to the satellite image and transect shown in Figure 2.

[22] Values of the ice crystal effective radius in clouds are derived from

$$r_e = \frac{3IWC}{2\rho_i\beta_{ext}} \quad (1)$$

[Foot, 1988], where  $IWC$  and  $\beta_{ext}$  are derived from bulk probe data rather than size distributions [Garrett et al., 2003], and  $\rho_i$  is the bulk density of ice.

[23] Gamma distributions of the form  $N = N_0 D^\mu \exp^{-\Lambda D}$  were fitted to particle size distributions (PSD) with diameters greater than  $50 \mu\text{m}$  for each  $1 \text{ km}$  of horizontal distance. The intercept  $N_0$ , slope  $\Lambda$ , and dispersion  $\mu$  were derived by matching the first, second, and sixth moments of the PSD. It is considered that this set provides the best fit over the entire measured particle size range [Heymsfield et al., 2002].

[24] We also examined the depletion of HDO relative to its theoretical concentration in the oceans. HDO has a slightly higher vapor pressure than  $\text{H}_2\text{O}$ . According to

Rayleigh distillation, if all condensate is assumed removed during adiabatic cooling, the fractionation of HDO ( $\delta\text{-HDO}$ ) should range from  $-86\%$  above the ocean to  $-950\%$  at the coldest tropopause. Measured values of  $\delta\text{-HDO}$  near the low-latitude tropopause during CRYSTAL-FACE were as low as  $-900\%$  [Webster and Heymsfield, 2003].

### 3.2. Observations

[25] Shown in Figure 5 are measurements taken along the length of the TTC cloud sampled on 21 July 2002. Both inside and outside the cloud, the air was supersaturated by 10 to 20% with respect to ice. Values of  $Q$  in the cloud were higher than in ambient air by up to 50%. The difference in  $Q$  was due to an extremely tenuous cloud of small but numerous ice crystals. Values of ice water content and extinction in the cloud layer were  $\sim 0.002 \text{ g m}^{-3}$  and  $< 1 \text{ km}^{-1}$ , respectively. Ice crystal concentrations were  $\sim 1 \text{ cm}^{-3}$  and the effective radius  $\sim 7 \mu\text{m}$ .

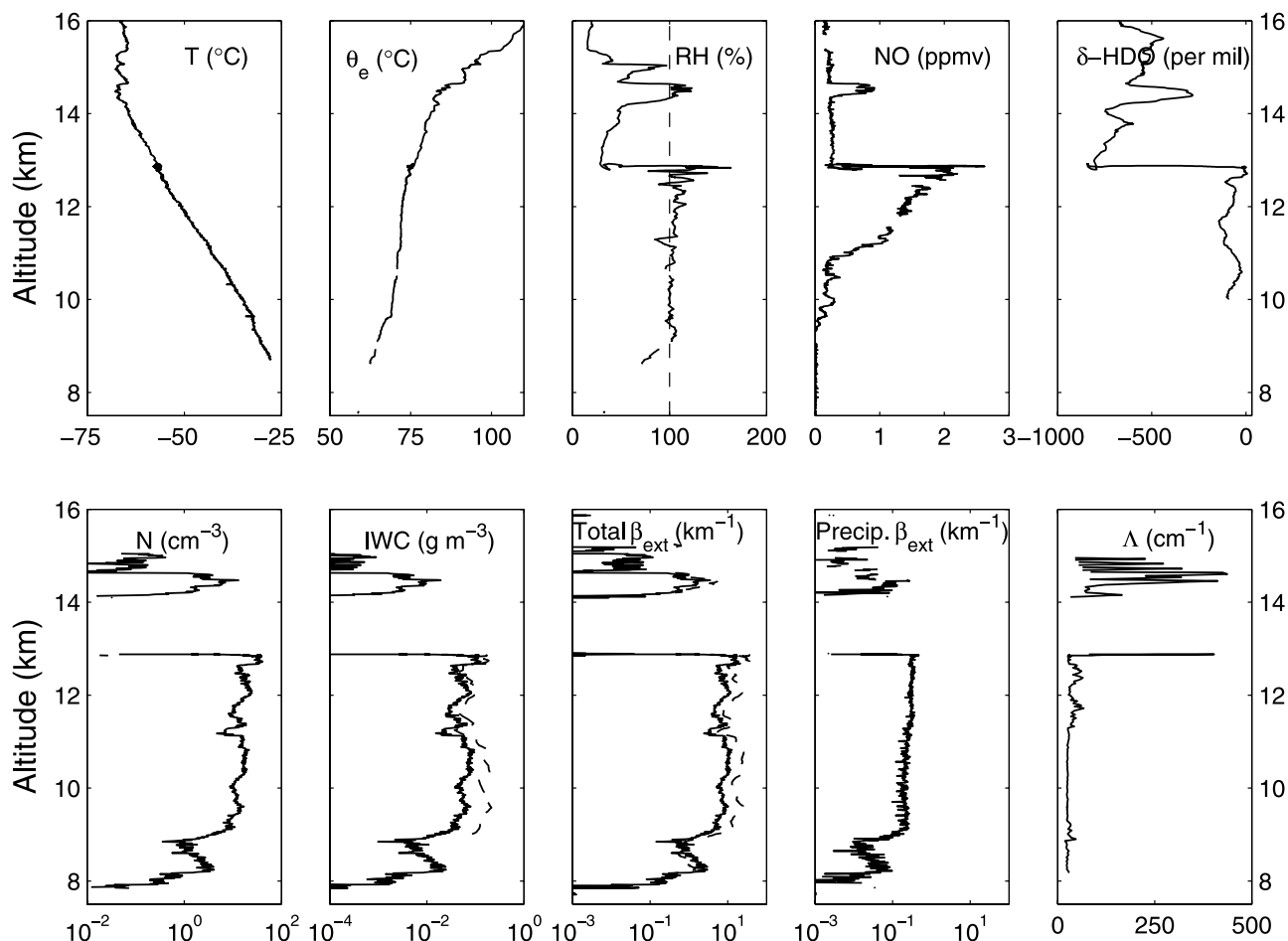


**Figure 6.** Profile of cloud during descent through an anvil on 28 July. In the bottom set of panels, curves with solid lines are derived from size distribution cloud probes, and dashed lines represent measurements from bulk cloud probes.

[26] In a different, much larger cloud system sampled on 28 July 2002, a descending profile was flown through the entire depth of a cirrus anvil (Figure 6). The anvil extended southwest over the southern Florida peninsula and was approximately two hours old when sampled. The system had two cloud layers, a highly stable TTC cloud above a comparatively well-mixed anvil cirrus layer. The TTC itself was separable into two layers. The lower layer extended from approximately 14.2 km to the lower bounds of the tropopause at 14.6 km, and the upper layer from 14.6 to 14.9 km.

[27] Temperatures in the lower TTC layer were depressed by  $\sim 3$  K from ambient temperatures, and the relative humidity was supersaturated by  $\approx 10\%$ . The cloud was only moderately tenuous; the optical depth was about 1, and maximum values of  $\beta_{\text{ext}}$  approached  $6 \text{ km}^{-1}$ . Precipitation-sized ice crystals in the layer were present but did not contribute significantly to the cloud opacity. Harvard water measurements of total water were not available in this cloud. *IWC* values were therefore derived from ALIAS total water and Harvard water vapor concentrations. Values of *IWC* reached a maximum of  $0.03 \text{ g m}^{-3}$  in the layer. The corresponding value of  $r_e$  derived from measurements of  $\beta_{\text{ext}}$  and *IWC* (equation (1)) is about  $10 \text{ }\mu\text{m}$ . Peak

concentrations of ice crystals larger than  $2 \text{ }\mu\text{m}$  diameter were  $13 \text{ cm}^{-3}$ .

[28] Therefore this layer, although tenuous, was characterized by high concentrations of small ice crystals. This microphysics is consistent with in situ formation from homogeneous nucleation of preexisting haze particles provided initial updraft speeds of  $0.5$  to  $1 \text{ m s}^{-1}$ , based on an analytical formulation derived by [Kärcher and Lohmann, 2002]. This formulation used estimations of the critical saturation ratio (aerosol activity) required for nucleation [Koop et al., 2000] to demonstrate that the number concentration of homogeneously nucleated ice crystals depends on updraft velocity and temperature alone.

[29] The second, higher TTC layer was just saturated with respect to ice, and was an order of magnitude more tenuous with peak concentrations of  $0.3 \text{ cm}^{-3}$ . These concentrations are consistent with updraft speeds of  $0.05 \text{ m s}^{-1}$  at the time of cloud formation. The *IWC* of the layer was just  $0.001 \text{ g m}^{-3}$ . The upper TTC layer may have been more tenuous than the lower TTC layer because it was located within in the tropopause, which had higher static stability.

[30] Beneath the TTC layers, separated by a vertical gap of  $1.2 \text{ km}$ , was the bulk of the anvil. The anvil was  $\sim 5 \text{ km}$  thick

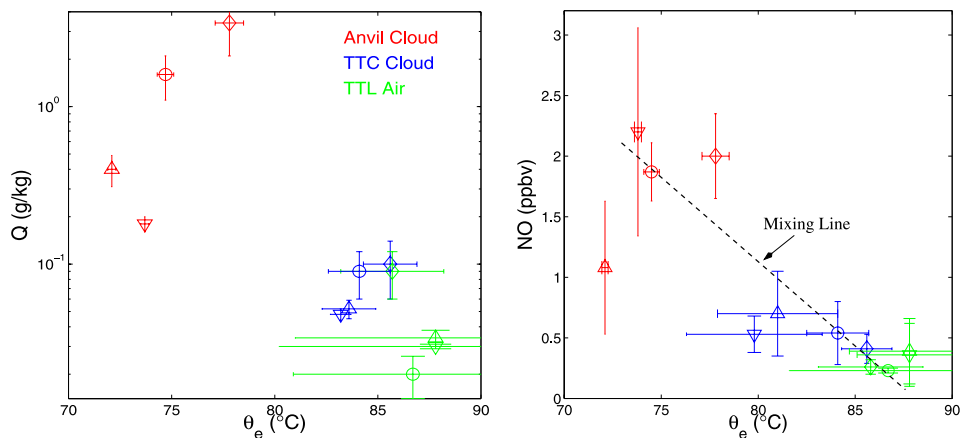


**Figure 7.** Measurements of NO and  $Q$  and equivalent potential temperature  $\theta_e$  in thin tropopause cirrus (TTC) cloud (blue), anvil cloud (red), and tropopause transition layer (TTL) air (green) with the same mean level as the TTC cloud, obtained on 16 and 28 July 2002. Clouds of the same system are paired by shape. Error bars show the standard deviation in the measurements during the averaging time period. A hypothetical NO linear mixing line is shown for illustration for a set of data points from 16 July.

with a cloud top temperature of  $-57^\circ\text{C}$ . The integrated optical depth derived from extinction measurements was  $\sim 64$ , with peak values of  $\beta_{ext}$  approaching  $40\text{ km}^{-1}$ .  $IWC$  and ice crystal number concentrations were approximately  $0.15\text{ g m}^{-3}$  and  $15\text{ cm}^{-3}$ , respectively. Values of  $r_e$  were  $\sim 8\text{ }\mu\text{m}$  at the anvil top, increasing to  $15\text{ }\mu\text{m}$  at the anvil base.

[31] Particularly notable is the NO profile. At high altitudes, NO is an identifier for deep convection, since it may either be created in situ by lightning, or carried undissolved from the polluted boundary layer. The primary sink for NO in the upper troposphere is photochemical oxidation to reservoirs like  $\text{HNO}_3$ . However, this timescale is on the order of days to weeks, which is much longer than the life cycle of the convective systems studied. Relative to upper tropopause air, enhanced NO concentrations were observed not only in the anvil cloud, but also in the lower (but not upper) TTC layer (Figure 6). Within TTC layers, it is unlikely that lightning is an in situ source for NO because these clouds are very thin and the ice crystals are probably too small to promote significant charge separation. Therefore the NO perturbation in the lower tropopause cirrus layer appears to indicate the TTC air had either mixed with or originated from deep convection.

[32] Figure 7 shows an intercomparison of  $Q$  and NO, and the ice phase equivalent potential temperature  $\theta_e$  from 16 July and 28 July. The measurements are categorized according to whether they were obtained within anvil cloud, the associated TTC layer, or nearby TTL air.  $\theta_e$  is approximately conserved under moist-adiabatic processes. Strictly, within deep convective clouds, NO and  $Q$  are not conserved because lightning and precipitation are often present. However, the sink for NO is negligible for the time scales of interest, and  $Q$  lacks a source. Thus the combination of  $\theta_e$ ,  $Q$ , and NO can be used to plot a mixing diagram from which the origins of tropopause cloudy air can be inferred.

[33] Figure 7 shows that values of NO,  $Q$  and  $\theta_e$  in the TTC are intermediate to those of anvil cloud and nearby

TTL air, and an approximate linear mixing line connecting the three groups of measurements can be drawn. The TTC data points are closer to TTL than anvil data points on these plots, which suggests that TTL air contributes most substantially to the properties of the TTC. However, there is a small but significant contribution from anvil (and thus convective) air also. Thus the tropopause cirrus appears to have formed primarily from high  $\theta_e$ , low NO and low  $Q$  air from near the tropopause, having incorporated small but nonnegligible contributions from convection. On the basis of mixing lines drawn through the data shown in Figure 7 we estimate the fractional contribution of convection to the TTC ranges up to 0.5.

[34] Additional evidence that tropopause cloud was formed in situ in the TTL, rather than from convective detrainment, comes from intercomparison of the depletion of heavy water vapor  $\delta\text{-HDO}$  within the cloudy air to the slope of the cloud particle size distribution  $\Lambda$ . An examination of exponential-type particle size distributions, fitted to particle probe data in midlatitude stratiform cloud systems by a number of researchers [Ryan, 2000], suggests that there is a nearly monotonic increase in the PSD slope with decreasing temperature. For convective cloud systems, a similar tendency was observed (Heymsfield et al., 2004, ms in review), but with considerably lower slopes noted in the ice cloud layers at similar temperatures. This tendency suggests that in an anvil cloud, for example, the regions formed by ice lofting from below can be differentiated from those produced in situ. This result was tested using the HDO measurements from CRYSTAL-FACE [Webster and Heymsfield, 2003], where the highest values of  $\Lambda$  were found in air with the highest fractionation of HDO.

[35] This is clearly illustrated in Figure 8, where we plot  $\delta\text{-HDO}$  and  $\Lambda$  for anvil and tropopause cloud in two convective systems measured on 28 July during CRYSTAL-FACE. Anvil cirrus had low values of  $\Lambda$ , indicative of precipitation sized ice crystals, and low (negative) values of  $\delta\text{-HDO}$  less than  $-100\text{‰}$ , indicative

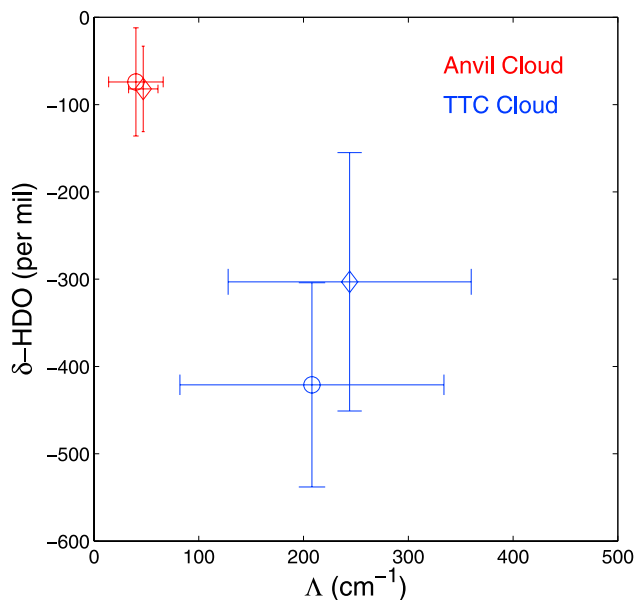


**Figure 8.** The  $\delta$ -HDO and size distribution slope parameter  $\Lambda$  obtained in tropopause cirrus cloud (blue) and corresponding anvil cloud (red) on 28 July. Where there is overlap, symbols correspond to the same clouds shown in Figure 7.

of lower troposphere air. In the tropopause cirrus, high values of  $\Lambda$  indicate a comparative absence of precipitation sized crystals, which suggests that tropopause cloud particles were not advected from lower altitudes but rather formed in situ. Values of  $\delta$ -HDO in the TTC, between  $-150$  and  $-550\text{‰}$ , were higher than the values between  $-600$  to  $-800\text{‰}$  observed in surrounding clear air. This picture is consistent with the air in the TTC having formed in the upper troposphere, but having mixed somewhat with convective air.

#### 4. Origins of Tropopause Cirrus

[36] What are the origins of the thin tropopause cirrus layer? At first glance, comparing the first and second flight passes shown in Figures 1a–1c, it appears that the generation of the upper layer was associated with convective cells that reached the tropopause at  $\sim 15$  km. It then seems plausible that the formation of the TTC might be attributed to detrainment of moist air from convection into the tropopause. This is the first hypothesis proposed by Jensen *et al.* [1996b]. The difficulty with this explanation is that, at least for the cases presented here, if the lower anvil shaped cloud is also due to detrained air, it is difficult to imagine how air might be detrained at its level of neutral buoyancy in two distinct layers, and not rather in a continuum. In fact, the TTC layer is much more stratified than the anvil and the potential temperature approximately 10 K higher. Further, this paper has shown mixing arguments based on thermodynamic and chemical tracer measurements in the TTC, as well as measurements of HDO depletion in tropopause cloudy air, that suggest that the air in TTC is derived primarily from the TTL, with only a minor contribution from convective air derived from lower altitudes.

[37] Alternatively then, the TTC might have existed prior to convective activity, having been formed by synoptic-scale uplift. This is the second viable source for tropopause cirrus proposed by Jensen *et al.* [1996b]. Here the TTC layers might have mixed somewhat with deep convection to become enriched with vapor and NO (Figures 5 and 7). However, if this were indeed occurring, it is hard to imagine how this is consistent with observations showing that the horizontal dimensions of the TTC layers studied were nearly identical to those of the anvil beneath (Table 1). Also, the concentrations of ice crystals in the TTC, if formed by homogeneous nucleation, are consistent with formation at updraft speeds between  $0.1$  and  $1 \text{ m s}^{-1}$  [Kärcher and Lohmann, 2002]. This is about an order of magnitude higher than the concentrations predicted for updraft speeds characteristic of gentle synoptic-scale uplift.

[38] Thus the TTC layers observed during CRYSTAL-FACE appear to have been created by convection but formed primarily in situ. If this is consistent with neither hypothesis proposed by Jensen *et al.* [1996b], what then are the origins of the TTC?

[39] Multilayered cirrus near convection have been observed previously at midlatitudes. Over the continental United States and Europe, plumes of cloud occasionally form in distinct layers above anvils that have been observed to emanate from domes of convection. These appear to be separable into two categories. Using stereo photography, Fujita [1982] observed that when a convective dome collapses violently, “jumping cirrus” may shoot back over it from a convergence zone just downwind. This cirrus is then advected down shear in a stratospheric layer distinct from the anvil. Such jumping cirrus has been seen near the tropopause quite often in time lapse photography of deep convection over the Great Plains, although it rarely lasts longer than several minutes (W. Lyons, personal communication, 2004).

[40] Alternatively, Levizzani and Setvák [1996], Setvák *et al.* [2003], and Wang [2003] have used multispectral satellite imagery to describe transparent plumes of cloud that spread over the anvil from a single circular source just several kilometers across. The plume is generally smaller in horizontal dimension than the anvil beneath it, and is usually sufficiently elevated to cast a shadow. Unlike, jumping cirrus, it does not shoot up from the anvil, but rather radiates from elevations comparable to the highest altitude of the convective dome. Comparisons of satellite imagery with radiative transfer simulations show that these plumes are composed of very small ice crystals with effective radii between  $4$  and  $7 \mu\text{m}$  [Melani *et al.*, 2003]. Setvák *et al.* [2003] speculated that a possible explanation for the circular source is that they are pileus clouds, stratiform cloud layers formed ahead of convective uplift.

[41] There is no conclusive evidence that either mechanism discussed by Fujita [1982] and Levizzani and Setvák [1996] plays a role in the Florida region. The cloud dynamics at midlatitudes might be closely analogous to those observed over mountain ridges since wind shear is typically high near the tropopause. By contrast, over Florida, wind shear at high altitudes is relatively low. However, like Setvák *et al.* [2003], we speculate that the TTC layers described here started as stratiform pileus clouds, forced upward by the deep convection. A photo-



**Figure 9.** Photograph taken from the WB-57F at  $\sim 18$  km altitude on 19 July 2002 during CRYSTAL-FACE (courtesy B. Barnett).

graph of a developing cumulonimbus tower seen from the WB-57F on 19 July 2002 shows a pileus cloud forming at the upper bounds of a deep convective turret. The pileus cloud was most optically dense at its upper bounds and in a thin vellum at the edge of the turret. In between, the sky was extremely transparent but nonetheless more visibly opaque than the deep blue sky above.

[42] Pileus clouds have been noted at high altitudes worldwide, at the tops of hurricanes [Bluestein and Marks, 1987], and both Great Plains and Tropical Warm Pool deep convection [Warner, 1984; Corfidi and Gayno, 1990]. They are similar to orographically forced clouds in that they are formed during isentropic uplift. However, unlike lee wave clouds, where the mountain is stationary, here the perturbation moves with the flow, i.e., it is the vertical motion of the obstacle rather than the horizontal motion of the air that creates the vertical displacement of stratified air. To our knowledge there has been no detailed analytical or numerical investigation into the dynamics behind their formation. As a guideline, in a stratified medium one would expect that the stability of the atmosphere would resist uplift ahead of the cloud. The vertical displacement of air ahead of a rising thermal  $\delta z$  can be inferred from a balance between the kinetic energy just above the thermal, and the potential energy due to the restoring force from atmospheric stratification

$$\delta z \sim \frac{W_{cloud}}{N} \quad (2)$$

where  $W_{cloud}$  is the rate of rise of the convective turret, and  $N$  is the buoyancy frequency below the tropopause. Considering that cirrus anvils detrain from deep convection at the level of neutral buoyancy, which was several kilometers below the tropopause during CRYSTAL-FACE, turrets near the tropopause are decelerating, and  $W_{cloud}$  is then probably significantly less than peak convective updraft velocities of  $\sim 10$  m/s. Given that  $N$  near the tropopause is  $\sim 0.01 \text{ s}^{-1}$ , then  $\delta z$  is on the order of several hundred meters.

[43] In fact, this estimate from scale analysis is in remarkably good accord with the  $\sim 200$  m vertical displacement seen in the gravity wave observed in tropopause cirrus measured on 21 July (Figure 4). Whether this displacement is sufficient to induce cloud formation depends on the initial level of moisture in TTL. The critical ice saturation ratio  $S_i$  at which ice particles homogeneously freeze is  $\sim 1.6$  at temperatures characteristic of the tropopause [Koop *et al.*, 2000]. For the 21 July case, the ambient ice saturation ratio was  $S_i \simeq 1.15$ , in which case the uplift required for homogenous freezing is about 300 m. Thus the observed amplitude of the gravity wave in the TTC downwind of the convection is similar to that required to induce condensation from TTL air.

[44] If the gravity wave perturbation shown in Figure 4 is induced by convection, its wavelength should be of similar magnitude to the size of the convective turret that pushes up against the TTL. The wavelength of the gravity wave observed in the TTC on 21 July was 2 km. This is probably close to the spatial scale of the largest turbulent eddy (or cumulus turret) seen in the example shown in Figure 9. Thus the horizontal and vertical scales of the gravity wave motions associated with this TTC layer are consistent with convective uplift of stratified air near the tropopause.

[45] If this convective uplift leads to formation of a pileus cloud, the pileus should disappear quickly once the convective forcing is removed and it relaxes to a level of subsaturation. This is unless the pileus layer is punctured by the convective updraft. In this event, the pileus persists and evolves to form an extensive stratiform sheet, even once the original convection has subsided. This has been observed in tropical Africa by Lacaze [1966] and Scorer [1972] and in France by Coulomb and Sourdillon [1944]. In fact, such ‘‘puncturing’’ appears to be occurring within the vellum of cloud over the cumulus shown in Figure 9. It is here, near the tropopause, that the convective cloud may mix with the stratiform cloud due to turbulent mixing. Subsequently, the stratiform pileus layer becomes sufficiently enriched with moisture as to remain cloudy in the downward phase of the wave (Figure 10).

[46] Arguably, such a process is shown in the first and second flight passes shown in Figures 1a–1c. On 23 July, deep convection forced air upward to 15.5 km, but once it had subsided to about 12 km, it left behind a long-lived stratiform cloud layer with tops at 15 km, below the highest altitude reached by the dome. Also, as shown in Figures 5 and 7, TTC clouds observed during CRYSTAL-FACE were enriched with total water and NO compared to nearby TTL air, in a manner consistent with them having mixed with convection. It is possible that the highest TTC layer shown in Figure 6, which was not enriched over the TTL in moisture, NO or HDO, had simply never been punctured by the convection.

[47] Some of these details have been simulated numerically by Wang [2003], who studied the formation of cirrus layers above Midwest severe thunderstorm anvils. Wang [2003] showed that gravity waves are formed just above deep convection in the stratosphere. These waves may form clouds vertically separate from the anvil, and similar in character to both types of tropopause cirrus observed by Fujita [1982] and Levizzani and Setvák [1996]. Wang [2003] noted that the displacement of isentropic surfaces by the waves would be expected to form clouds only

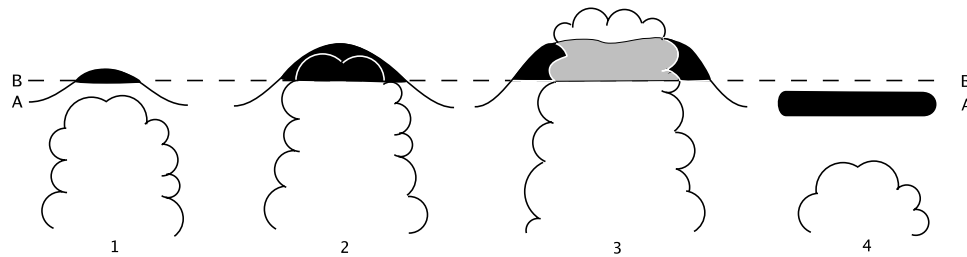


**Figure 10.** Illustration of a pileus formation hypothesis for TTC. A TTL stable layer at A has its condensation level at B just below the tropopause. In stage 1 a cumulonimbus turret forces air at level A upward, and some is lifted above level B to form a pileus cloud (black shading). In stage 2 the pileus grows to form a cap over the top of the turret. If the turret is sufficiently vigorous, it may penetrate the stable layer and mixing may occur between the pileus and the cumulonimbus (gray shading, stage 3). Once the cumulonimbus turret subsides to its level of neutral buoyancy, the pileus must relax to level A (stage 4). The pileus is now enriched with moisture from the cumulonimbus turret, so a new stratiform cloud layer forms [cf. Scorer, 1972].

temporarily. However, in some of his simulations, the waves were sufficiently vigorous to break, entraining “gulps” of moist dome or anvil air, thereby promoting the formation of long lived plumes of high-altitude cirrus. Wang [2003] proposed that such moisture enriched tropopause clouds provided a mechanism for increasing the water vapor content of the stratosphere. Wang [2003] noted that less vigorous turbulent mixing may also be generated by simple shear between the rising convective cloud and its environment [Grabowski and Clark, 1991, 1993]; this weaker mechanism also generated enhanced tropopause humidities in his model. Here Figures 1a–1c, 4, and 9 appear more consistent with this less vigorous process. Waves are not breaking. Rather, turbulent mixing may be occurring between the pileus layer and the cumulonimbus tower either because of interfacial wind shear, or firm suppression of convection by the tropopause. Whatever mechanism is responsible for the mixing, both observations and numerical simulations suggest that convectively induced gravity waves can propagate within stratiform cloud sheets.

[48] Once a stratiform layer is formed it might spread and thicken (Figures 1a–1c) due to radiatively induced cooling. Hartmann *et al.* [2001] showed that if a cold and thick anvil layer is present beneath a TTC layer, the TTC will be shielded from the hot earth’s surface, and cool throughout its depth. For the example of TTC observed during CRYSTAL-FACE on 21 July, when the anvil was sufficiently thick to be a blackbody, Garrett *et al.* (submitted manuscript, 2004) calculated instantaneous heating rates in the TTC layer of  $-0.2$  K/day. These increased to 1 K/day as the anvil thinned to an optical depth of 2. Thus one would expect TTC layer on 21 July to thicken after initial formation, but then dissipate once the anvil had thinned. As illustrated for the 23 July case also shown in Figures 1a–1c, this did not in fact occur. Observations of Tropical Western Pacific cirrus anvils have shown TTC layers persisting for days following a convective event [Comstock *et al.*, 2002].

## 5. Summary

[49] Here we have presented aircraft observations from the CRYSTAL-FACE field program showing that thin tropopause cirrus (TTC) layers are frequently observed about 1 km above cirrus anvils. These TTC were long-

lived, optically tenuous, and composed of very small ice crystals with effective radii less than  $10 \mu\text{m}$ . Thus their microstructures were similar to those observed in tropopause cirrus widespread over much of the globe. The mechanism for the production of these clouds at low latitudes has been debated. The leading theories suggest that they are either generated by gravity waves propagating vertically upward from convection into the stratosphere [e.g., Potter and Holton, 1995], large-scale synoptic uplift near the tropopause, or that they are the remnants of anvil detrainment [Jensen *et al.*, 1996b].

[50] The observations from CRYSTAL-FACE show that none of these theories can entirely account for the formation of TTC layers above cirrus anvils. Tropopause cirrus appeared to have been derived from ambient tropopause air that had mixed with air from within deep convection. The locations of TTC, and their chemical, physical and thermodynamic properties, were clearly distinct from those of the anvil. The TTC do not appear to have been remnants of anvil detrainment.

[51] However, neither did the TTC appear to be formed by synoptic-scale uplift, particularly as their horizontal scale was nearly identical to that of the anvil layer beneath. The TTC contained a strong signature of a 2 km wavelength gravity wave with an amplitude of about 200 m. Similarly, Potter and Holton [1995] showed in numerical simulations that gravity waves induced by deep convection can propagate into the lower stratosphere to form clouds. In their study, however, the lengths of the waves were much longer than those seen here, and the clouds appeared only in the upward phase, upwind of the convection, and not in a continuous stratiform layer downwind of the convective dome.

[52] The observations presented here suggest that the TTC layers observed above anvils originate as pileus clouds formed as deep convection pushes upward stably stratified air near the tropopause. Accordingly, they contain a monochromatic gravity wave signature with a wavelength similar to the dimension of the largest convective turrets that formed them. In the upward phase of the wave the air is displaced upward by several hundred meters, which is sufficient to form a cloud provided that initially the TTL air is sufficiently moist. They do not evaporate in the downward phase of the wave because the convection is

sufficiently vigorous that the pileus layer is punctured by the moist convective dome. This provides opportunity for mixing between the pileus cloud and deep convection, enriching the stratiform layer with moisture and trace gases.

[53] The mechanism by which the pileus layer then evolves to become a widespread stratiform sheet (as shown in a beautiful series of photographs by *Scorer* [1972]) is uncertain. However these thin layers can be cooled radiatively by the thick anvil beneath [*Hartmann et al.*, 2001; *Comstock et al.*, 2002; *Garrett et al.*, submitted manuscript, 2004], and this will tend to drive deepening and spreading of the pileus layer. The above mechanism bears closest resemblance to numerical simulations done by *Wang* [2003] which show tropopause cirrus formation over anvils forced by Great Plains storm cells.

[54] We emphasize that the above hypothesis is speculative, and does not preclude other mechanisms from playing an important role in the formation of some tropopause cirrus layers. Even over the Florida region, extremely tenuous ( $\beta_{ext} \simeq 0.05 \text{ km}^{-1}$ ) and widespread thin tropopause cirrus were observed on 13 July that appeared to have formed in the absence of convective influence (*E. Jensen et al.*, Formation of a tropopause cirrus layer observed over Florida during CRYSTAL-FACE, submitted to *Journal of Geophysical Research*, 2004). The cloudy air mass had not encountered deep convection for at least one day prior. Rather, modeling results showed that the cirrus was driven by rapid temperature oscillations due to high-frequency gravity waves.

[55] The convectively associated tropopause cirrus layers presented here were much more persistent than the anvil layers beneath them. Thus they provided for a thermodynamically stable source of extremely cold and widespread cirrus near the tropopause. If their longevity was due to convection, they provides a mechanism for transport of air enriched in vapor and trace gases to the upper tropopause, above the level of neutral buoyancy where anvil cloud would normally be detrained. Rather than contributing to the freeze-drying of the TTL, as would be the case if they precipitated and had formed entirely in situ due to synoptic-scale uplift, TTC clouds may in some cases be an earmark for TTL moistening. Since the TTL is cold, and both ice crystals and water vapor are strongly absorbing at infrared wavelengths, the pileus hypothesis proposed here would suggest a convective mechanism for widespread radiative heating in the TTL.

[56] Testing this hypothesis will require more detailed observations of TTC clouds above anvils, both near the convection itself and far downwind. Photographs have shown that pileus clouds form near the tropopause. Numerical simulations should be able to explicitly reproduce tropopause pileus formation, in which case they may shed light on how such tropopause cloud layers evolve.

[57] **Acknowledgments.** This work was supported by the NASA CRYSTAL-FACE mission. L. Nguyen and P. Minnis provided satellite data products used in this study. Elliot Weinstock provided Harvard water data. E. Zipser and E. Jensen gave useful suggestions. Appreciation is due to the flight crews of the NASA WB-57F and ER-2.

## References

Baumgardner, D., H. Jonsson, W. Dawson, D. O'Connor, and R. Newton (2002), The cloud, aerosol and precipitation spectrometer (CAPS): A new instrument for cloud investigations, *Atmos. Res.*, *59*–*60*, 251–264.

- Bluestein, H. B., and F. D. Marks Jr. (1987), On the structure of the eyewall of Hurricane Diana (1984): Comparison of radar and visual characteristics, *Mon. Weather Rev.*, *115*, 2542–2552.
- Boehm, M. T., and S. Lee (2003), The implications of tropical Rossby waves for tropical tropopause cirrus formation and for the equatorial upwelling of the Brewer-Dobson circulation, *J. Atmos. Sci.*, *60*, 247–261.
- Comstock, J. M., T. P. Ackerman, and G. G. Mace (2002), Ground-based lidar and radar remote sensing of tropical cirrus clouds at Nauru Island: Cloud statistics and radiative impacts, *J. Geophys. Res.*, *107*(D23), 4714, doi:10.1029/2002JD002203.
- Corfidi, S. F., and G. A. Gayno (1990), Some visual observations on the development of a plains mesoscale convective system, *Weather Forecast.*, *5*, 172–180.
- Coulomb, J., and M. Sourdillon (1944), Nuages coiffant la montagne d'air froid formée sous un orage, *Ann. Geophys.*, *1*, 92–95.
- Dessler, A. E., and P. Yang (2003), The distribution of tropical thin cirrus clouds inferred from Terra MODIS data, *J. Clim.*, *16*, 1241–1247.
- Foot, J. S. (1988), Some observations of the optical properties of clouds, part 2, Cirrus, *Q. J. R. Meteorol. Soc.*, *114*, 145–164.
- Fujita, T. T. (1982), Principle of stereoscopic height computations and their application to stratospheric cirrus over severe thunderstorms, *J. Meteorol. Soc. Jpn.*, *60*, 355–368.
- Garrett, T. J., H. Gerber, D. G. Baumgardner, C. H. Twohy, and E. M. Weinstock (2003), Small, highly reflective ice crystals in low-latitude cirrus, *Geophys. Res. Lett.*, *30*(21), 2132, doi:10.1029/2003GL018153.
- Gerber, H., Y. Takano, T. J. Garrett, and P. V. Hobbs (2000), Nephelometer measurements of the asymmetry parameter, volume extinction coefficient, and backscatter ratio in clouds, *J. Atmos. Sci.*, *57*, 3021–3034.
- Grabowski, W. W., and T. L. Clark (1991), Cloud-environment interface instability: Rising thermal calculations in two spatial dimensions, *J. Atmos. Sci.*, *48*, 527–546.
- Grabowski, W. W., and T. L. Clark (1993), Cloud-environment interface instability, part II: Extension to three spatial dimensions, *J. Atmos. Sci.*, *50*, 555–573.
- Hartmann, D. L., J. R. Holton, and Q. Fu (2001), The heat balance of the tropical tropopause, cirrus, and stratospheric dehydration, *Geophys. Res. Lett.*, *28*, 1969–1972.
- Heymsfield, A. J. (1986), Ice particles observed in a cirriform cloud at  $-83^{\circ}\text{C}$  and implications for polar stratospheric clouds, *J. Atmos. Sci.*, *43*, 851–855.
- Heymsfield, A. J., A. Bansemer, P. R. Field, S. L. Durden, J. L. Stith, J. E. Dye, W. Hall, and C. A. Grainger (2002), Observations and parameterizations of particle size distributions in deep tropical cirrus and stratiform precipitating clouds: Results from in situ observations in TRMM field campaigns, *J. Atmos. Sci.*, *59*, 3457–3491.
- Jensen, E. J., O. B. Toon, L. Pfister, and H. B. Selkirk (1996a), Dehydration of the upper troposphere and lower stratosphere by subvisible cirrus clouds near the tropical tropopause, *Geophys. Res. Lett.*, *23*, 825–828.
- Jensen, E. J., O. B. Toon, H. B. Selkirk, J. D. Spinhirne, and M. R. Schoeberl (1996b), On the formation and persistence of subvisible cirrus clouds near the tropical tropopause, *J. Geophys. Res.*, *101*, 21,361–21,375.
- Jensen, E. J., W. G. Read, J. Mergenthaler, B. J. Sandor, L. Pfister, and A. Tabazadeh (1999), High humidities and subvisible cirrus near the tropical tropopause, *Geophys. Res. Lett.*, *26*, 2347–2350.
- Kärcher, B., and U. Lohmann (2002), A parameterization of cirrus cloud formation: Homogeneous freezing including effects of aerosol size, *J. Geophys. Res.*, *107*(D23), 4698, doi:10.1029/2001JD001429.
- Koop, T., B. Luo, A. Tsias, and T. Peter (2000), Water activity as the determinant for homogeneous ice nucleation in aqueous solutions, *Nature*, *406*, 611–614.
- Lacaze, J. (1966), Remarques sur les pileus, *J. Rech. Atmos.*, *4*, 487–488.
- Levizzani, V., and M. Setvák (1996), Multispectral, high-resolution satellite observations of plumes on top of convective storms, *J. Atmos. Sci.*, *53*, 361–369.
- Li, L., G. M. Heymsfield, P. E. Racette, L. Tian, and E. Zenker (2004), A 94 GHz cloud radar system on a NASA high-altitude ER-2 aircraft, *J. Atmos. Oceanic Technol.*, in press.
- Luo, B. P., et al. (2003), Dehydration potential of ultrathin clouds at the tropical tropopause, *Geophys. Res. Lett.*, *30*(11), 1557, doi:10.1029/2002GL016737.
- Massie, S., A. Gettelman, W. Randel, and D. Baumgardner (2002), Distribution of tropical cirrus in relation to convection, *J. Geophys. Res.*, *107*(D21), 4591, doi:10.1029/2001JD001293.
- McFarquhar, G. M., A. J. Heymsfield, J. Spinhirne, and B. Hart (2000), Thin and subvisual tropopause tropical cirrus: Observations and radiative impacts, *J. Atmos. Sci.*, *57*, 1841–1853.

- McGill, M. J., D. L. Hlavka, W. D. Hart, V. S. Scott, J. D. Spinhirne, and B. Schmid (2002), The cloud physics lidar: Instrument description and initial measurement results, *Appl. Opt.*, *41*, 3725–3734.
- McGill, M. J., L. Li, W. D. Hart, G. M. Heymsfield, D. L. Hlavka, P. E. Racette, L. Tian, M. A. Vaughan, and D. M. Winker (2004), Combined lidar-radar remote sensing: Initial results from CRYSTAL-FACE, *J. Geophys. Res.*, *109*, D07203, doi:10.1029/2003JD004030.
- Melani, S., E. Cattani, F. Torricella, and V. Levizzani (2003), Characterization of plumes on top of deep convective storm using AVHRR imagery and radiative transfer simulations, *Atmos. Res.*, *67–68*, 485–499.
- Minnis, P., D. P. Garber, D. Young, R. F. Arduini, and Y. Takano (1998), Parameterizations for reflectance and emittance for satellite remote sensing of cloud properties, *J. Atmos. Sci.*, *55*, 3313–3339.
- Pfister, L., et al. (2001), Aircraft observations of thin cirrus clouds near the tropical tropopause, *J. Geophys. Res.*, *106*, 9765–9786.
- Potter, B. E., and J. R. Holton (1995), The role of monsoon convection in the dehydration of the lower tropical stratosphere, *J. Atmos. Sci.*, *52*, 1034–1050.
- Prabhakara, C., R. S. Fraser, G. Dalu, C. W. Man-Li, and R. J. Curran (1988), Thin cirrus clouds: Seasonal distribution over oceans deduced from Nimbus-4 IRIS, *J. Appl. Meteorol.*, *27*, 379–399.
- Ridley, B., et al. (2004), Convective transport of reactive constituents to the tropical and mid-latitude tropopause region: I. Observations, *Environ.*, *38*, 1259–1274.
- Ryan, B. F. (2000), A bulk parameterization of the ice particle size distribution and the optical properties in ice clouds, *J. Atmos. Sci.*, *57*, 1436–1451.
- Sandor, B. J., E. J. Jensen, E. M. Stone, W. G. Read, J. W. Waters, and J. L. Mergenthaler (2000), Upper tropospheric humidity and thin cirrus, *Geophys. Res. Lett.*, *27*, 2645–2648.
- Santacesaria, V., et al. (2003), Clouds at the tropical tropopause: A case study during the APE-THESIO campaign over the western Indian Ocean, *J. Geophys. Res.*, *108*(D2), 4044, doi:10.1029/2002JD002166.
- Scorer, R. (1972), *Clouds of the World*, Stackpole Books, Harrisburg, Pa.
- Scott, S., T. P. Bui, K. R. Chan, and S. W. Bowen (1990), The meteorological measurement system on the NASA ER-2 aircraft, *J. Atmos. Ocean. Technol.*, *7*, 525–540.
- Setvák, M., R. M. Rabin, C. A. Doswell III, and V. Levizzani (2003), Satellite observations of convective storm tops in the 1.6, 3.7 and 3.9  $\mu\text{m}$  spectral bands, *Atmos. Res.*, *67–68*, 607–627.
- Spang, R., G. Eidmann, M. Riese, D. Offermann, P. Preusse, L. Pfister, and P.-H. Wang (2002), CRISTA observations of cirrus clouds around tropopause, *J. Geophys. Res.*, *107*(D23), 8174, doi:10.1029/2001JD000698.
- Sunil Kumar, S. V., K. Parameswaran, and B. V. Krishna Murthy (2003), Lidar observations of cirrus cloud near the tropical tropopause: General features, *Atmos. Res.*, *66*, 203–227.
- Wang, P. K. (2003), Moisture plumes above thunderstorm anvils and their contributions to cross-tropopause transport of water vapor in midlatitudes, *J. Geophys. Res.*, *108*(D6), 4194, doi:10.1029/2002JD002581.
- Warner, C. (1984), Stereo-pair photographs of monsoon clouds, *Bull. Am. Meteorol. Soc.*, *65*, 344–347.
- Webster, C. R., and A. J. Heymsfield (2003), Water isotope ratios D/H,  $^{18}\text{O}/^{16}\text{O}$ ,  $^{17}\text{O}/^{16}\text{O}$  in and out of cloud map dehydration pathways, *Science*, *302*, 1742–1745.
- Webster, C. R., R. D. May, C. A. Trimble, R. G. Chave, and J. Kendall (1994), Aircraft (ER-2) laser infrared absorption spectrometer (ALIAS) for in-situ stratospheric measurements of HCl, N<sub>2</sub>O, CH<sub>4</sub>, NO<sub>2</sub>, and HNO<sub>3</sub>, *Appl. Opt.*, *33*, 454–472.
- Weinstock, E. M., et al. (1994), New fast response photofragment fluorescence hygrometer for use on the NASA ER-2 and the Perseus remotely piloted aircraft, *Rev. Sci. Instrum.*, *65*, 3544–3554.
- Winker, D. M., and C. R. Trepte (1998), Laminar cirrus observed near the tropical tropopause by LITE, *Geophys. Res. Lett.*, *25*, 3351–3354.

---

D. G. Baumgardner, Centro de Ciencias de la Atmosfera, Universidad Nacional Autonoma de Mexico, Mexico City, DF 04510, Mexico.

T. P. Bui, NASA AMES Research Center, Moffett Field, CA 94035, USA.

T. J. Garrett, Meteorology Department, University of Utah, 135 S 1460 E, Room 819, UT 84112, USA. (tgarrett@met.utah.edu)

A. J. Heymsfield and B. A. Ridley, National Center for Atmospheric Research, PO Box 3000, Boulder, CO 80307-3000, USA.

M. J. McGill, Goddard Space Flight Center, Code 912, Greenbelt, MD 20771, USA.

C. R. Webster, Earth and Space Sciences Division, Jet Propulsion Laboratory (JPL), California Institute of Technology, Pasadena, CA 91109, USA.